HiSST: 3rd International Conference on
High-Speed Vehicle Science & Technology
14-19 April 2024, Busan, Korea

An exploration of adjoint-based optimization for hypersonic vehicle- and propulsion design.

Carola Rovira Sala [*1], Marc Famada Vizcaino [†1, 3], Alberto Simon Felix [1], Ambara Bernabeu-Vazquez [‡3], Bart Van Hove [§4], Tamás István Józsa [¶1], and Jimmy-John O.E. Hoste [‖3]

[1]Centre for Computational Engineering Sciences, School of Aerospace, Transport and Manufacturing, Cranfield University
[3]Destinus SA, Switzerland
[4]Destinus Spain S.L.

Abstract

The design of hypersonic vehicles and hypersonic propulsion systems is a challenging endeavor. Affordable large-scale computational systems have made CFD more accessible, including for optimization related tasks. Adjoint optimization methods, that were previously in the realm of research, are now available in commercial software. This work explores the use of adjoint-based optimization for hypersonic vehicle design in two case studies on external and internal hypersonic flows using a commercial CFD software. For the external flow problem, lift over drag is maximised for a waverider geometry while considering various constraints. In the internal flow case, proxy measures of mixing efficiency are maximised to improve combustion efficiency inside a hydrogen scramjet geometry using adjoint CFD. Both the advantages and the limitations of adjoint-based optimization are evaluated.

Keywords: *adjoints, waverider, scramjet*

1. Introduction

1.1. Historial perspectives

Hypersonic vehicles have been a subject of interest in the past century with the first manned atmospheric hypersonic flight achieved in the X-15 program in 1961 [1]. Hypersonic vehicles could enable access-to-space in single-stage-to-orbit (SSTO) space planes [2] or reduce significantly intercontinental flight times. Accomplishing this is a technological challenge, as exemplified by the National Aerospace Plane (NASP) program back in the late 1980s. NASP was a US program to develop an SSTO hydrogen aircraft with airbreathing propulsion. These hypersonic vehicles have to support high heat and mechanical loads and must be coupled with highly integrated propulsion systems. Interest in such a program was sparked by successful subscale scramjet tests, and by significant advances in Computational Fluid Dynamics (CFD) as well as in structures and heat-resistant materials [3]. While progress in hypersonic product development was clear, in order to bring diverse technologies to a level of maturity sufficiently high to realize such a program had proven to be an important hurdle. It led to the cancellation of the program in 1994.

Since the NASP era, CFD has gained an important place in general hypersonic vehicle design, especially in the last decade, which has been boosted by a more widespread availability of computational power with relative affordability. This development has made CFD a powerful tool to complement wind tunnel and flight testing. This trend is observable in the literature of the past two decades with hypersonic flight test programs such as the X43 [4], X51 [5], HyShot [6], HIFiRE [7], IXV [8, 9] and the more

[*] *Currently Research assistant, DLR, Cologne, Germany*
[†] *CFD engineer*
[‡] *Combustion engineer*
[§] *Head of Advanced Programs*
[¶] *Lecturer in Computational Fluid Dynamics*
[‖] *Aerothermodynamics and Combustion engineer*

recent BOLT program [10, 11]. Moreover, commercial softwares have matured now offering users a wide variety of solvers for different applications as well as design methods including adjoint-based optimization. The growing availability of adjoint CFD solvers has also been observed in the CFD vision 2030 report [12, 13]. The number of studies on the application of adjoint-based optimization on supersonic [14] and hypersonic [15] design problems remains limited. The present study set out to investigate the applicability of adjoint-based optimization, readily available in the commercial software STAR-CCM+ [16], on high-speed internal and external aerodynamics problems related to hypersonic vehicle design. The shape designs of a waverider geometry and a hydrogen combustor were identified as relevant test cases.

One of the challenges of hypersonic vehicles is the aeroshape design itself with an ideal shape dictated by each flight regime. The most efficient aeroshape for hypersonic vehicles in terms of lift over drag ratio (L/D) is the waverider, where pressure created by the shock wave below the vehicle is used for lift boosting. This requires an aircraft geometry that is tailored specifically to interact with the surrounding shock field. The corresponding shape tends to be slender with sharp edges but is, however, not suited for subsonic or supersonic flight as illustrated in [17]. Waveriders are historically designed through stream-tracing methods, relying on analytically derived (basic) inviscid flow fields [18, 19, 20, 21]. Additional features such as propulsion flowpaths require careful consideration to avoid negative interaction with other design features. An important disadvantage of the state-of-the-art semi-analytical methodology is that it provides geometries optimized for single Mach numbers based on inviscid flow assumption. It is an open question whether adjoint CFD methods could be leveraged in hypersonic vehicle design to relax the aforementioned limitations.

On the air-breathing propulsion side, scramjet technology, where the flow remains supersonic throughout the whole internal flow path, has been identified as the enabling technology for hypersonic flight. Improving mixing and combustion efficieny in scramjets is extremely challenging (see e.g., [22, 23]), but crucial in making their use to propel hypersonic vehicles viable. A parallel wall injection strategy, such as in the experiment of Burrows and Kurkov [24], has the advantage of cooling the wall through the fuel but has a very limited mixing capability. A transverse injection mechanism such as in the HyShot II [25] has a higher penetration depth but induces higher total pressure losses due to the jet obstruction. Shock waves and shock wave boundary layer interactions are flow features that can have a positive or negative impact on scramjet mixing and combustion. Adjoint-based CFD could potentially help design supersonic combustors.

The aim of this work is to quantify the achievable benefits of adjoint-based optimization in hypersonic design problems. To this end, both external and internal aerodynamics problems are considered using a commercial CFD software. The investigated case studies cover the optimization of a hypersonic waverider geometry and the optimization of a supersonic hydrogen combustor. Subection 1.2 provides a brief overview on the use of adjoint optimization in the literature for engineering design problems.

1.2. Literature review on adjoint-based optimization

This Section discusses the use of adjoint-based CFD methods in the general context of aerospace (see 1.2.1) as well as specific to field of hypersonics (see 1.2.2).

1.2.1. The adjoint method in aerodynamic shape optimization

As introduced above, several technologies can benefit from aerodynamic shape optimization. Optimization is the process of finding the best solution to a given problem [26]. In complex optimization problems, finding the optimal solution is challenging or even impossible. Nevertheless, in shape optimization problems, even if the optimal design is not achieved, obtaining an improved design is still extremely valuable from an engineering perspective.

Various optimization methods exist in the context of aerodynamic shape optimization. Some of the most extensively used in the aerospace sector are gradient-based methods. The latter rely on the information about the gradient of the objective function with respect to the design variables to guide the optimization. This characteristic provides them a greater scalability compared to gradient-free methods, which makes them well suited for problems with tens or even hundreds of design variables.

However, for large number of design variables, the evaluation of sensitivities becomes increasingly more computationally expensive. A solution to this shortcoming is to use the adjoint method to compute such sensitivities, since its computational cost is shown to be linearly proportional to the number of variables [27]. Adjoint-based aerodynamic shape optimization is applied to numerous fields in the aerospace sector, given that the optimization problems usually present a small number of objective functions and a large number of design variables.

The adjoint-based aerodynamic shape optimization of airfoils is extensively studied [28, 29, 30, 31, 32, 33, 34, 35], because of the relatively simple problem definition and the usefulness of the optimized designs for aerospace applications. Furthermore, adjoint-based methods have also been successfully applied to three-dimensional wings [36, 37, 38] as well as turbomachinery blades. Regarding the optimization of compressor blades, for instance, the feasibility of the method to increase the efficiency, while maintaining the mass flow rate and stagnation pressure ratio, has been demonstrated [39, 40]. Other related works can be found in [41, 42, 35, 43].

Adjoint-based optimization is present in multi-disciplinary optimization problems. Most common optimization problems feature aero-structure optimization, such as the high-fidelity aero-structural design optimization framework applied to wing design [44], the torque maximisation in wind turbine blades [45], or the aero-structural design optimization of a wing with flutter constraints [46]. Other authors include acoustics in the optimization, such as in [47], where an aero-structural-acoustic optimization framework is designed for noise signature reduction in rotorcraft problems. Furthermore, the MADELEINE European project [48] exemplifies a general interest in adjoint-based multidisciplinary optimizations for industrial configurations.

With regard to mixing and combustion, adjoint-optimization has not been widely explored. One of the difficulties is the need to specify an adjoint equation for each species which can't be easily generalized. A way to circumvent this is by relying on a passive scalar transport equation. This method has been adopted by Mosca *et al.* [49] in a T-mixer geometry and by Eggl *et al.* [50] in a stirring device. Another analysis [51] was conducted in a 2D channel under subsonic conditions to optimize the uniformity of particle distribution in the outlet, validating the strategy with numerical differentiation and quantifying the reduction on the calculation cost compared to traditional methods. Finally, the adjoint-based design optimization of vortex generators has been investigated for an inlet under subsonic and transonic conditions, with a focus in enhancing the flow quality entering the engine [52, 53]. This methodology can be potentially used to maximize mixing efficiency in the supersonic combustor of a scramjet.

1.2.2. Adjoint-based optimization in relation to hypersonics

To some extent, adoint-based CFD methods have been applied in hypersonic design. The large interest in this discipline and the increased complexity of wind-tunnel testing, create the perfect conditions for developing innovative optimization tools in both external and internal aerodynamics.

This paragraph provides a concise review on the application of adjoint-based optimization in external aerodynamics. Hypersonic waverider optimization using adjoint-based methods has not been extensively studied, but several articles show their potential. An example of this is the multi-disciplinary optimization of the parameterized geometry of a waverider-derived hypersonic vehicle in terms of aerodynamics, structure and trajectory [54]. Other approaches considered the optimization of a similar waverider-derived hypersonic vehicle for lift-constrained drag minimization under a constant volume geometrical constraint [55]. Another article explored the optimization of a hypersonic waverider geometry in terms of aerodynamic efficiency for a wide speed range, showing an increase in the latter at low speeds, while maintaining an excellent performance at cruise conditions [56].

This paragraph provides a concise review on the application of adjoint-based otpimization in relation to internal aerodynamics. Scramjet intake design optimization was investigated in [57], where the geometry was first parameterized using Free Form Deformation (FFD) and then optimized for maximum mass flow rate in several operating conditions. A posterior investigation by the same authors [58] demonstrated multi-objective optimization of the same scramjet inlet geometry with respect to thrust and nozzle exit

area. A similar approach was used to optimize a hypersonic inlet to have a uniform pressure distribution across the throat of the inlet while maintaining a compression ratio of 2 across the cowl shock [15].

To the authors' knowledge, adjoint CFD methods have not yet been applied to the study of hypersonic propulsion systems. The present work aims at exploring the possibility to do so for supersonic mixing optimization problems.

2. Methods

In order to assess the capability of the adjoint-based optimization, a generic waverider geometry (Subsection 2.2) and a supersonic combustor (Subsection 2.3) are selected. Section 2.1 describes the adjoint-based optimization strategy for both test cases. The employed software is STAR-CCM+ [16].

2.1. Adjoint-based optimization

In the present study, optimization problems are considered targeting to minimize a cost function denoted by J. The cost function depends on the real valued ($\mathbb{R}^n$) collection of position vectors ($\vec{x}_b$) characterising the discrete points representing the boundary region (curve in 2D, surface in 3D) subject to modification. Considering an initial configuration described by $\vec{x}_b^{\text{ini}}$, a modified configuration can be obtained with displacement vectors $\vec{\delta}$ so that $\vec{x}_b^{\text{mod}} = \vec{x}_b^{\text{ini}} + \vec{\delta}$. Thereafter, the optimization problems investigated here can be described as

$$\min_{\vec{\delta} \in \mathbb{R}^n} \; J(\vec{x}_b^{\text{ini}}, \vec{\delta}). \tag{1}$$

Case-specific cost functions and constraints are detailed in Sections 2.2 and 2.3.

The adjoint-based optimization procedure used to solve the problem defined by Eq. (1) is depicted in Figure 1. Starting from a baseline geometry, flow field computation is carried out to determine the value of the cost function. Thereafter, the scalar-valued sensitivity field S is computed. S is defined as the derivative of the cost function to be minimized with respect to the local surface-normal displacement.

Next, displacements are computed from the sensitivity field with Eq. (2) where the total displacement $\vec{\delta}$ is obtained as

$$\vec{\delta} = \vec{\delta}_c + f_c S \vec{n}. \tag{2}$$

Here, $\vec{\delta}_c$ is the cumulative displacement from the corresponding iteration, f_c is a collection of factor functions applied to the sensitivity S to constrain the movement around the geometry and to preserve the boundaries, and $\vec{n}$ is the normal vector of the surface directed towards the fluid. The second term on the right-hand side of Eq. (2) is responsible for constraining the displacement field. For example, displacements perpendicular to symmetry boundary conditions need to be gradually damped to zero to preserve the flow configuration and only modify no-slip walls. Also, displacements computation often relies on the local averaging of the sensitivity field to avoid the propagation of numerical oscillations to the geometry. Finally, the displacement vector computed at the optimized surface is diffused to every grid point to provide a smooth displacement vector field for updating the mesh and thus the baseline geometry. The described procedure is suitable to carry out local optimization finding alternative configurations with decreased costs in the vicinity of the baseline configuration.

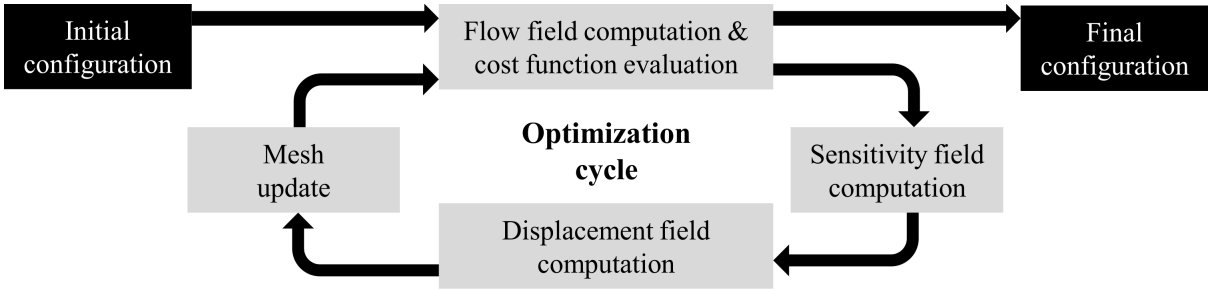

Fig 1. Schematic of the employed adjoint-based optimization procedure.

Table 1. Freestream conditions for waverider simulations.

Mach	h [km]	p_∞ [Pa]	T_∞ [K]	rho_∞ [kg/m^3]	U_∞ [m/s]	mu_∞ [Pa s]
8	30.5	1114	227	0.017	2416	$1.476 \cdot 10^{-5}$

2.2. Waverider bottom surface optimization

2.2.1. Flow configuration

For the external hypersonic test case, the bottom surface of a waverider is considered. As shown in Figure 2, only half of the surface is modelled by exploiting symmetry. Cone-derived waverider geometries are generated with an open-source code [59]. A freestream Mach number of 8 is considered corresponding to 30 km altitude matching part of the operating conditions of waveriders. Flow conditions are summarized in Table 1.

2.2.2. Formulation of the optimization problem

The examined optimization problem targets aerodynamic efficiency maximization – defined as the ratio of the lift L and drag D forces – while somewhat preserving cargo volume. The corresponding cost function is

$$J(\vec{\delta}) = -L/D \quad \text{while}\, V \geq c_V \cdot V_{initial} \tag{3}$$

Here, V and $V_{initial}$ are the volume of the optimized geometry and the initial volume, respectively. The c_V coefficient controls the reduction of the initial volume allowed during the optimization. With $c_V = 0$, the volume constraint vanishes.

The computed surface sensitivities are smoothed based on the inbuilt Gaussian filter of STAR-CCM+ [16]. The displacement field is constrained to avoid unwanted deformations (e.g., at the boundaries). To this end, the following filter as a function of a single parameter s is employed.

$$f(s) = \begin{cases} 0 & \text{if } s \leq FD \\ 1 - \left(\frac{2}{2FD-2TD} \cdot s + \frac{2TD}{2FD-2TD} \right)^{20} & \text{if } FD < s < TD - FD \\ 1 & \text{if } s \geq TD - FD, \end{cases} \tag{4}$$

where TD is the total distance covered by the filter and FD defines the distance from the boundary within which the displacement is fixed to zero (see [60]). The filter function $f(s)$ is part of the f_c factor in Eq. (2) which includes other filters as well.

2.2.3. Numerical solution methods

Simulations rely on the steady-state solver of Star-CCM+ [16]. Inviscid fluxes are treated with the improved advection upstream splitting method (AUSM+) with flux vector splitting (FVS) [61]. Spatial derivatives are discretized using a second-order scheme. Further details are described in [60, 62].

2.3. Supersonic parallel combustor optimization

2.3.1. Flow configuration

For the internal flow problem, the supersonic (non-)reacting wall jet experiment of Burrows and Kurkov [24, 63] is adopted. The popularity of this experiment, shown in Figure 3, follows from an extensive set of experimental and simulation data in both non-reacting and reacting conditions. The experimental setup consists of hydrogen injected parallel to a vitiated air-stream behind a backward facing step. Two different stages are simulated, a first one where there is only mixing of the species (H_2, H_2O and N_2) and a second one where the combustion takes place introducing O_2 and initialising with the first stage solution. Further details of the simulation strategy such as inflow conditions and reaction mechanisms are summarized in [64].

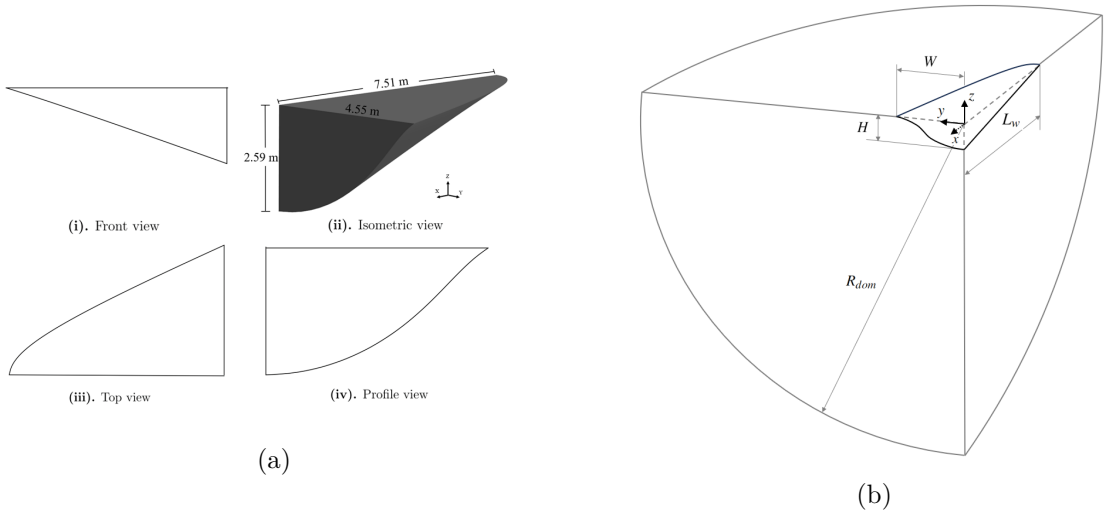

Fig 2. Cone-derived waverider geometry (a) views and (b) computational domain.

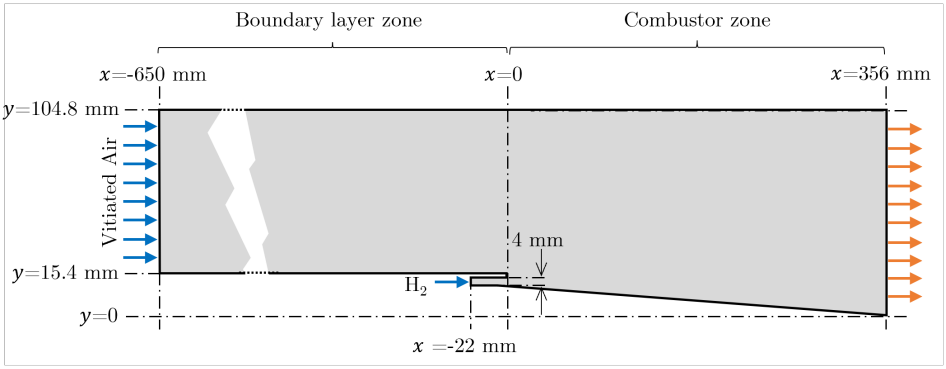

Fig 3. Schematic of the Burrows-Kurkov supersonic combustion experiment [24]. Not to scale.

2.3.2. Formulation of the optimization problem

Diverse strategies can be adopted to improve mixing, with different levels of obstruction. A possible implementation is to introduce an immersed obstacle at the mixing interface of the hydrogen and air streams. Another possibility is to add a less intrusive mounted obstacle to the wall in front of the injector. Both strategies have been considered in [64] and results for an optimized mounted obstacle are reported here. In addition, a setup where the diverging wall section is allowed to deform freely is also explored. In order to enhance mixing, the optimization problem is set to maximize the variance of hydrogen at the outlet of the domain with the following cost function:

$$J(\vec{\delta}) = -\mathrm{Var}\left(c_{H_2}^{\mathrm{out}}\right) \tag{5}$$

Here $\mathrm{Var}(c_{H_2}^{\mathrm{out}})$ is the variance of the hydrogen concentration at the outlet of the combustor.

Additionally, some constrains to the displacements resulting from the sensitivities computed will be imposed. For the optimized triangle, only the hypotenuse side will be able to move freely, and the vertical cathetus can only move in the vertical direction. This maintains the displacement between the length of obstacle and does not extend to the lower wall of the combustor. On the contrary, for the optimization of the lower wall, the only restriction was the horizontal position, between 80 mm and 300 mm. Previous analysis not presented here revealed that obstacles between these coordinates have the most positive impact on the outlet concentration [64].

2.3.3. Numerical solution methods

Similarly to the waverider case, the steady-state solver of Star-CCM+ is used. Inviscid fluxes are treated with the AUSM+ with FVS [61] and a second-order spatial discretization scheme. Turbulence is modeled with Menter's SST-2003 approach [65] and the default modeling settings. In analogy with other CFD studies in the literature [49, 50], a passive scalar strategy is used in order to use adjoint-based optimization in a mixing problem. The adjoint-based optimization of multispecies flow problems was not implemented in the employed version of STAR-CCM+ (version 2302) yet when this study was carried out. The passive scalar transport equation for the fuel concentration is

$$\mathbf{u} \cdot \nabla(\rho c_{\mathrm{H_2}}) = \nabla \cdot (\mathrm{j}_D \nabla c_{\mathrm{H_2}}). \tag{6}$$

Here, $\mathbf{u}$ is the velocity vector, $c_{\mathrm{H_2}}$ is the concentration of hydrogen and $\mathrm{j}_D = \frac{\mu}{Sc} + \frac{\mu_t}{Sc_t}$ is the linear eddy diffusivity with μ being the dynamic viscosity, Sc the Schmidt number and the subindex t denotes turbulent quantities.

Modeling the mixing stage with a passive scalar entails differences in the flow field. Compared to the multispecies simulation with fuel injection, thermophysical properties of the flow are not influenced by passive scalar concentration. For this reason, the x-velocity profiles along different the combustor differ in the case of the multispecies and passive scalar simulation cases as depicted in Figure 4. Shear layers near the wall ($y < 3$ cm) are present in both cases but the profiles differ clearly, even though passive scalar simulations have been set up with the same properties as the multispecies simulations with matching inflow conditions. Note that the injector boundary conditions in the passive scalar case have been adapted in order to match the total pressure profiles of the multispecies simulations and the experiments in the reactive case. In spite of the depicted differences in shear layer evolution, passive scalar simulations were found useful approach because some benefits of the identified favourable geometries translated to multi-species flow simulations.

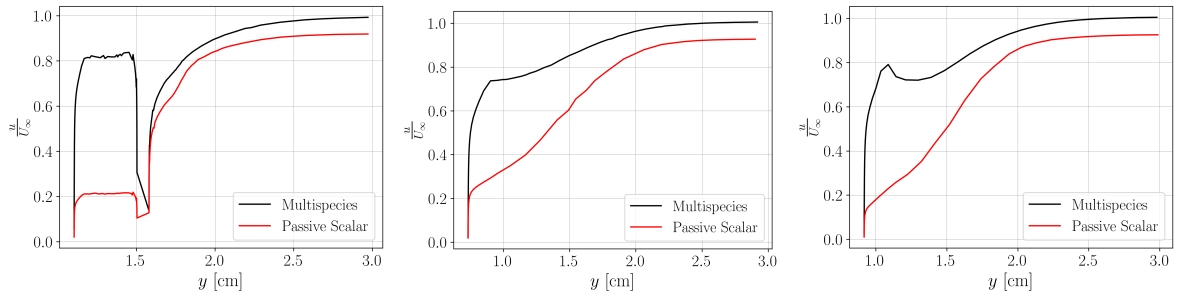

(a) (b) (c)

Fig 4. Comparison of the velocity profiles in the x direction between the mixing stage with multispecies and passive scalar strategy at (a) $x = 0$ mm, (b) $x = 60$ mm and (c) $x = 120$ mm.

3. Results and Discussion

This section presents the results of the different optimization problems with adjoint-based CFD. Subsection 3.1 covers the external hypersonic flow and Subsection 3.2 discusses the supersonic combustor.

3.1. Waverider optimization

A two step approach has been considered. Firstly, adjoint-based optimization is explored with inviscid simulations. Secondly, viscous optimizations are studied.

3.1.1. Inviscid optimization

Focus is placed on the inviscid optimization of a cone-derived waverider (20 degree cone angle) with dimensions shown in Figure 2 (a) (see also [62]). The length is taken in analogy to the X-51 waverider [5]. Various optimization constraints are explored based on the directions in which the surface is allowed to evolve as summarized in Table 2. Free optimization allows both the inward and outward displacement of

the waverider surface as dictated by the sensitivity field. Inward/outward optimization permits displacements solely in one direction with inward corresponding to shrinking the waverider volume. Depending on the strategy, an increase in L/D is obtained through a decrease in both lift and drag. Moreover, volume changes are measured as expected. The inward optimization is characterized by a relative improvement of L/D of 17% at the cost of a relative volume reduction equal to 10%. Figure 5 presents the deformed geometries, considering different stopping criteria related to the volume. The deformation procedure, especially visible in the XZ plane, makes use of expansion and compression waves in order to achieve its goal.

Table 2. Mach 8, inviscid waverider optimization.

	Original geometry	**Free optimization**	**Inward optimization**	**Outward optimization**
Lift (kN)	232.1	147.8	158.4	224.2
Drag (kN)	88.0	49.4	51.2	86.9
L/D (-)	2.63	2.99	3.09	2.58
Volume (m^3)	21	18.97	18.86	21.37

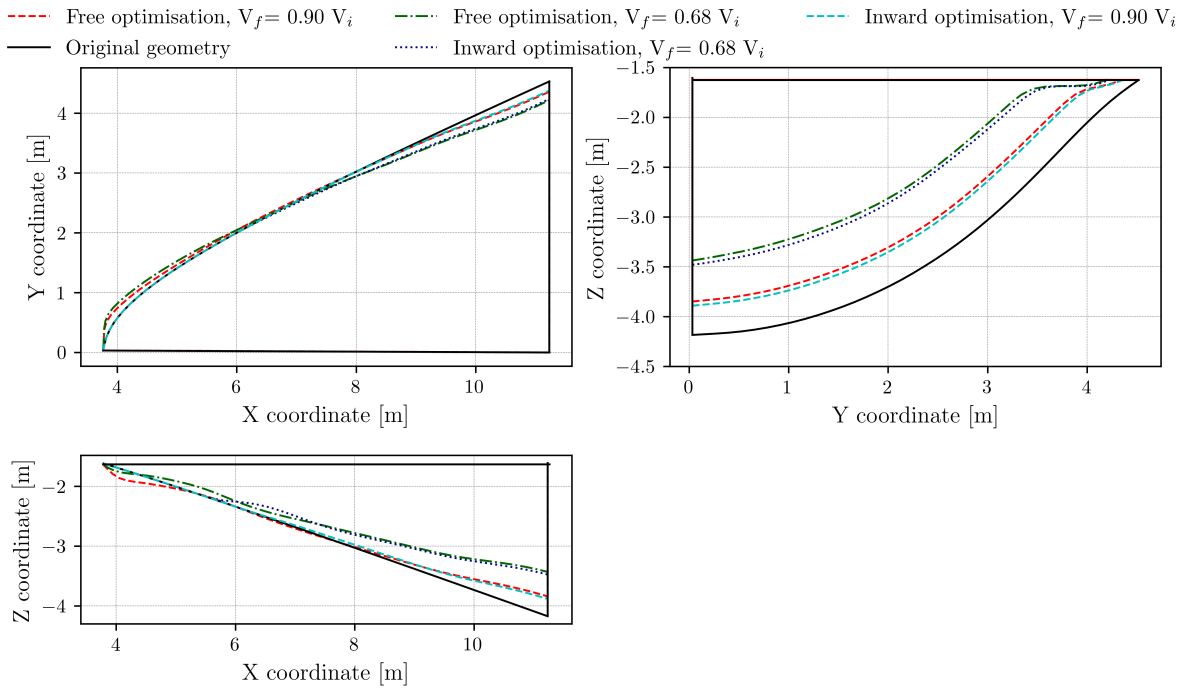

Fig 5. Final deformations of the inviscid optimized waveriders at Mach 8.

3.1.2. Viscous optimization

Next, viscous optimizations of cone-derived hypersonic waveriders are considered (see also [60]). The bottom surface of waveriders is designed such that the bow shock produced by the body remains attached throughout the leading edge in inviscid flow. This prevents any flow spillage to the upper surface and enhances aerodynamic efficiency by means of compression lift. However, in viscous flows, the interaction of the boundary layer with the shock detaches the latter from the leading edge, yielding a non-optimal geometry. Historically, methods to account for viscous effects in the shape derivation have been devised [20]. In the present study, adjoint-based optimization is tested as an alternative method to obtain reasonable viscous shapes starting from inviscid cone-derived geometries.

Waverider geometries are generated from the inviscid flow field around cones of semi-angle θ using horizontal slicing. The dimensions of the resulting geometries are gathered in table 3 and visualized in figure 2.

Table 3. Cone-derived waverider properties: cone semi-angle (θ), length (L), width (W), height (H).

θ [deg]	L [m]	W [m]	H [m]
4	10.0	2.00	0.51
7	10.0	2.56	1.05
11	10.0	3.51	1.77
20	10.0	6.05	3.43

Before proceeding to the optimization, the previous baseline geometries are analysed for inviscid and viscous flows at Mach 8. Figure 6 presents the results from these preliminary analyses in terms of lift-to-drag ratio and internal volume of the vehicle. The inviscid geometry generation method does not yield an optimal geometry in the considered range of θ listed in Table 3. The aerodynamic efficiency increases with the decrease of θ. Based on these results, the unconstrained optimization can be expected to evolve towards thinner geometries. This increase is obtained at the expense of the volume, which confirms that volume constraints must be applied to obtain geometries suitable for practical applications.

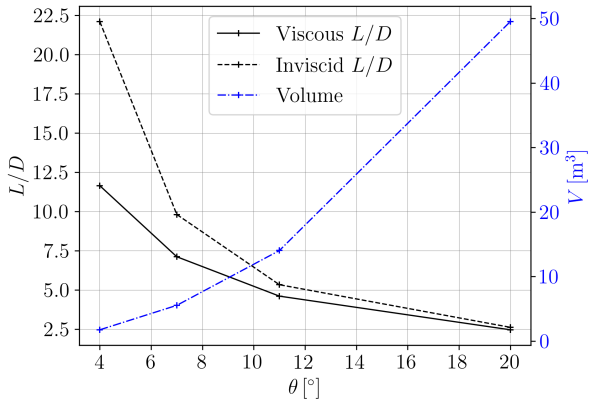

Fig 6. Lift-to-drag ratio of baseline waverider geometries and internal volume.

In a *first optimization approach*, the optimization is solely constrained with zero displacements at the symmetry and top planes. This is accomplished by introducing a function in the displacement computation that tends to zero near the boundaries as established in Eq. (2). Using this approach, a reduction of the angle of the lower surface and the subsequent reduction of the frontal area of the vehicle is obtained, as illustrated in figure 7. The optimized shapes share some similarities to the inviscid optimization which does make sense as the hypersonic aerodynamics are dominated by shock waves. The improved geometry achieves a considerable decrease in lift and an even greater reduction of drag, which translates into an increase of the lift-to-drag ratio of 21%. However, this improvement in aerodynamic efficiency is achieved at the expense of the volume. This result confirms the trend that was presented in figure 6.

A *second optimization approach* is devised to avoid undesirable volume reduction. A volume constraint is added by using a penalty method based on the deviation from a target volume, i.e. the initial volume. This method is able to increase the lift-to-drag ratio in 7.33% with a volume reduction of only 0.36%. See figure 8. Figure 9 compares the flow field around the baseline and the improved geometries by means of virtual Schlieren photography. A region with a high density gradient is found in the vicinity of the bottom surface of the waverider, i.e. the boundary layer. Furthermore, a semicircular region with high

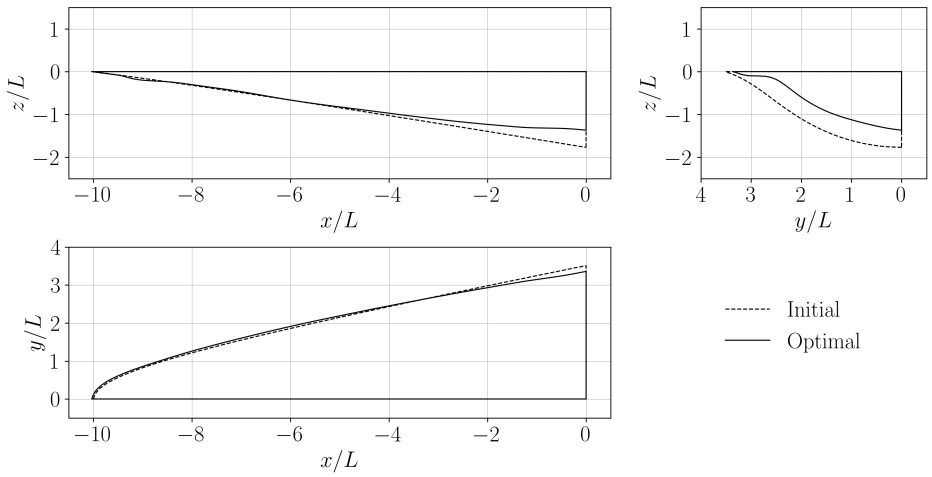

Fig 7. Side, front and top views of the baseline and optimized geometry with geometric constraints.

density gradient can be observed, corresponding to a bow shock wave. A slight change in curvature and symmetry axis vertical end point appears to be sufficient to keep similar bow shock characteristics. Such type of results would not be achievable without adjoint-based optimization.

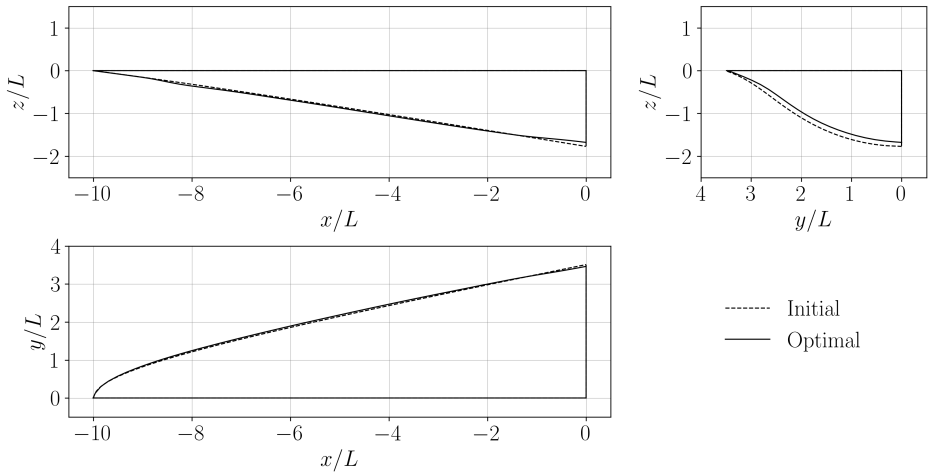

Fig 8. Side, front and top views of the baseline and optimized geometry with geometric and volume constraints.

3.2. Scramjet mixing optimization

Figure 10 reports the validation of simulations with experimental data in the case of the reference geometry (referred to as baseline case) for both mixing and combustion stages. Further details of the validation are provided in [64]. In general, a good agreement is found, with predictions similar to what has been reported in the literature [66]. The same mixing and combustion configurations are used for the adjoint-based optimization simulations.

Figure 11 (d) demonstrates the limitations of parallel injection. Mixing is limited to a thin region elongated in the streamwise direction, and fuel does not reach deeper layers of the air stream. Two different optimization cases are investigated to compare them with the baseline case. The first optimization case proposed is by introducing a mounted obstacle to enhance the mixing of the species (referred to as optimized triangle case). Different shapes and positions were analysed as mentioned previously, leading into an initial triangle shape to be optimized. The second optimization case allows the lower wall of the

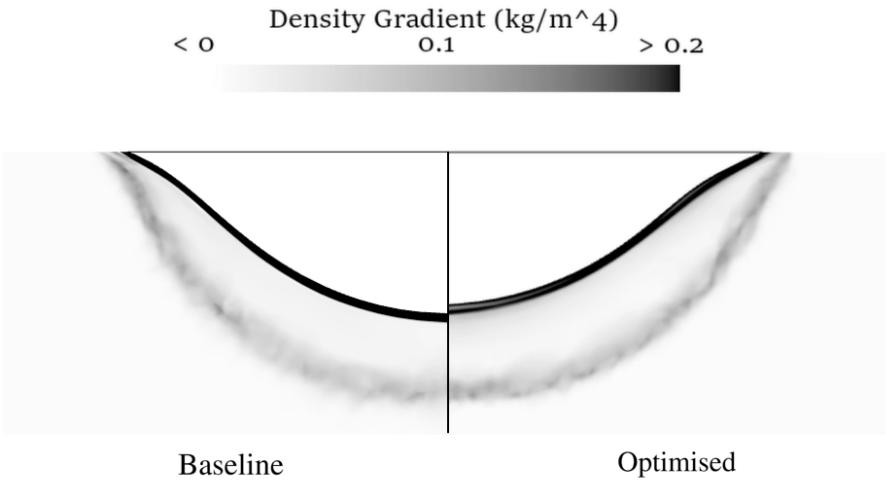

Fig 9. Flow field comparison using virtual Schlieren. Front view.

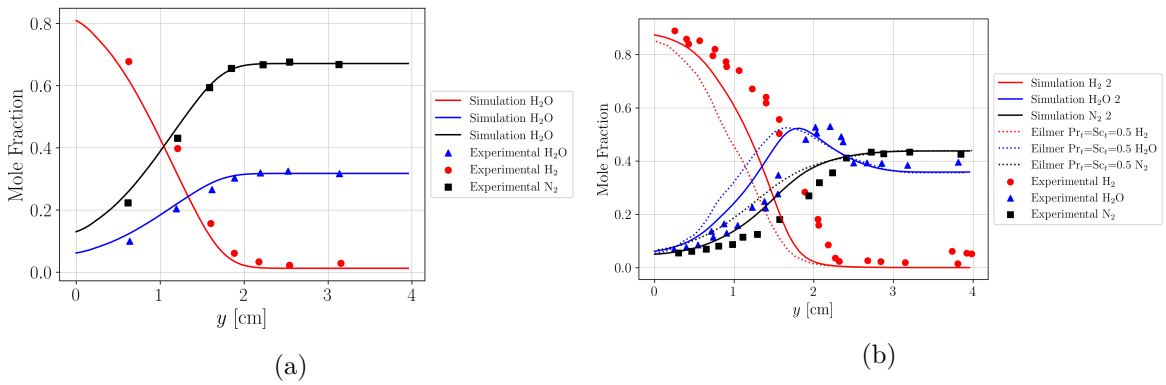

Fig 10. Mole fraction at the outlet for the (a) non-reacting and (b) reacting combustor setup. The experimental data and Eilmer simulation results correspond to [24, 63] and [66], respectively.

combustor to deform freely, in order to explore other potential strategies to improve mixing (referred to as optimized wall case). The optimized geometries are then used in a reacting setup with the same boundary conditions as the baseline case.

The comparative contour plots of the results are presented in Figure 11 for the various cases in the reacting stage. Clear differences with respect to the baseline case are visible. The optimized triangle shape presents a more hyperbolic shape on the hypotenuse side, smoother top vertex and increased in height driven by the intention of moving the H_2 to higher velocity zones. By doing so, increased hydrogen concentration is secured at the outlet. Similarly, the free wall optimization leads to a lower wall geometry elongated by hills and valleys. The free wall optimization suggests that multiple obstacles with smooth geometrical changes along the combustor wall can boost mixing efficiency. The resulting configuration is specific with well-defined hill heights and distances separating the heights which would be challenging to determine otherwise.

Furthermore, for both cases, the reaction zone behaves as for the baseline with similar ignition onset as observed in Figures 11 (d-i). The deformed wall stretches and widens the reaction zone downstream from the ignition point thus influencing both mixing and combustion efficiency. Additionally, the virtual Schlieren contours in Figures 11 (j-l) show the presence of various new shocks induced by the obstacle,

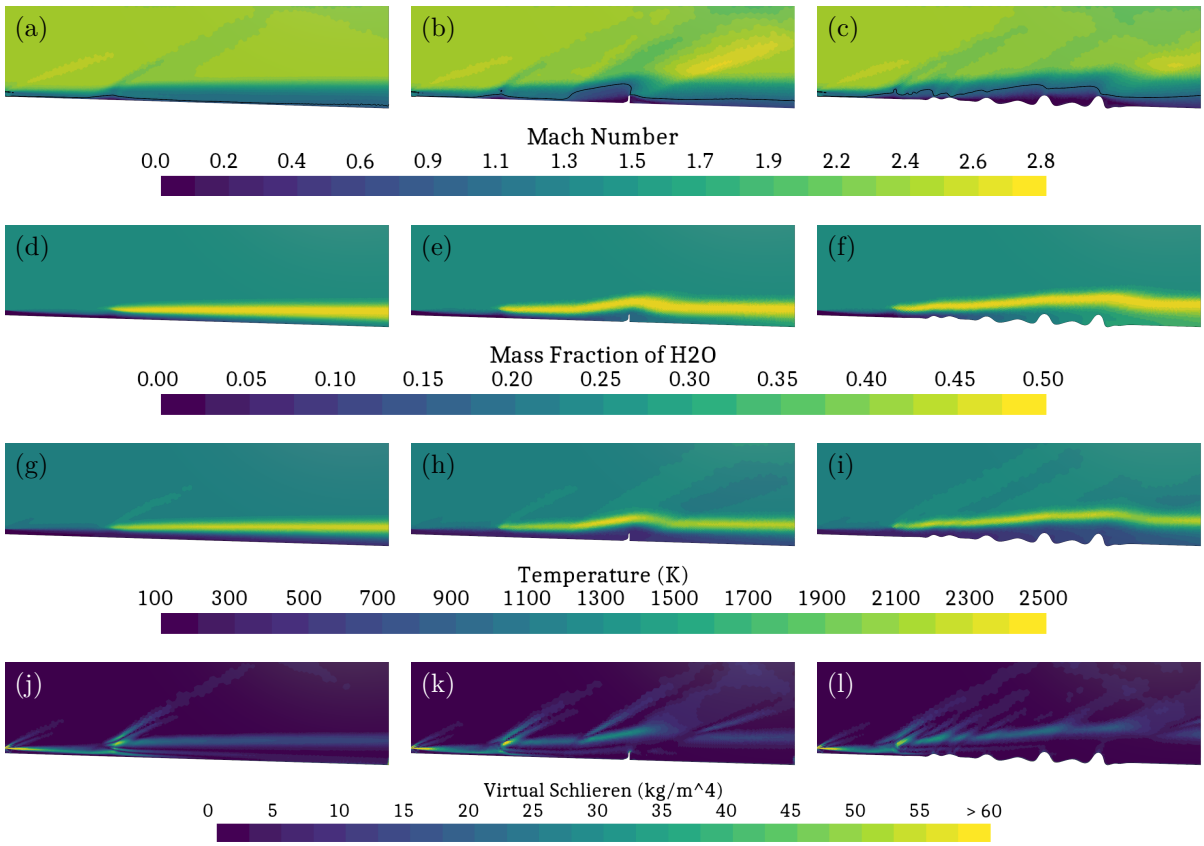

Fig 11. Contour plots of field variables in the reacting case: baseline simulation (left column), optimized triangle (middle column), and optimized wall (right column). Mach number with an isoline at Ma = 1 (a-c); H_2O mass fraction (d-f); Temperature (g-i); virtual Schlieren (j-l). The field of view covers the region between the injector outlet and the domain outlet.

which impact the total pressure losses across the combustor.

Figure 12 presents the comparison of the both mixing and reacting stages for the main variables used in the optimization. A clear effect of the optimization on the outlet concentration of hydrogen is shown, with an increase of its variance of around 15% for the optimized obstacle and more than double for the wall optimization. Therefore, the optimization conducted reached the objective imposed on maximising the variance of H_2 on the outlet of the mixing stage. The increase of mixing efficiency supports this optimization, where higher values of this variable correspond to higher variance, with an increase of 10% for the wall case (see Table 4). Additionally, the mixing stage results presented, indicate that the use of a passive scalar to model H_2 in the optimization is potentially beneficial for this type of setup.

When looking at how the modified geometry affects the combustion stage, the improvements are not as noticeable in the case of the optimized triangle. The variance of the product of the reaction (H_2O) does increase together with the combustion efficiency but only around 2% in the best case. In Figure 12, the effect of the obstacles in the combustion efficiency is depicted with a sharp increase of the variable after the position of the optimized triangle (200 mm) as opposed to the continuous increase in the baseline case. Overall, a strongly mixing limited combustion is still observed. However, combustion in the optimized wall case shows promising improvement even in the reacting stage. The benefit of the optimized wall manifests into an increased combustion efficiency peaking at 21.8% at the outlet. By comparison, the maximum combustion efficiency in the baseline case is 19.9% so that the optimization results in a 9.5% overall improvement as detailed in Table 4. The optimized wall case results in a substantially elongated reaction zone thanks to the hills and valleys introduced by the adjoint-based optimization. Figure

		Baseline	Optimized triangle	Optimized wall
Mixing efficiency [%]	*Maximum*	73.0	79.0	83.6
Combustion efficiency [%]	*Maximum*	19.9	20.4	21.8
Total pressure loss [%]	*Mixing stage*	5.62	7.88	7.50
	Combustion stage	9.00	11.3	11.1

Table 4. Comparison between baseline and optimized cases for efficiency and pressure loss for both stages

12 indicates that the combustion efficiency increases monotonically in the combustor as the vertical extent of the reaction zone grows with the streamwise distance. Logically, the optimizations suggest that elongating the reaction zone is crucial to enhance mixing and combustion efficiencies when parallel injection is employed.

Table 4 also provides the relative total pressure loss along the combustor, allowing to evaluate the penalty of the introduction of the obstacles. For both stages, the increment in pressure loss is around 2% for the best case. In the mixing stage this appears to be acceptable given the 10% efficiency increment. However, in the reacting stage, the improvement in combustion efficiency is comparable to the losses. In order to see an improvement of the combustion, further optimization including some combustion flow field related criteria should be explored. As pointed out previously, the version of STAR-CCM+ presently used does not allow for adjoint-based methods for a reacting flow.

4. Conclusions

Initial exploration has demonstrated the maturity of adjoint-based methods in STAR-CCM+ for general design purposes given its relatively simple usage when considering full surface mesh deformations. In general terms, results for waverider L/D maximization show a tendency to reduce lift slightly and drag more considerably, which increases the lift-to-drag ratio. This reduction is achieved at the cost of the vehicle's internal volume. For example, inviscid optimization led to a configuration with 17 % higher L/D compared to the baseline geometry, but the volume dropped by about 10 %. Hence, appropriate constraints to the volume must be applied. These initial results suggest that inviscid optimization could be used to improve waverider geometries in off-design conditions, while viscous optimization could assist to adapt the theoretically optimal waveriders in inviscid flow to real, viscous flows.

Regarding the mixing enhancing, adjoint-based method together with passive scalar transport delivered two design with an increase of the variance of the fuel concentration at the outlet. It is clear that with more deformation restrictions, the improvement is less noticeable (as seen in the triangle case) than when leaving more freedom. However, unconstrained optimization might result in configurations that are challenging to manufacture. Nevertheless, the optimization of the wall presents insights on the case that can be used for a more accurate optimization. Substantial improvement in combustion efficiency was found only when a relatively large part of the combustor wall was altered. This resulted in a combustion efficiency of 21.8 % compared to the baseline 19.9 %. The improvement in combustion efficiency was accompanied with a decrease in total pressure loss which grew from 9.0 % in the baseline case to 11.1 % in the optimized case suggesting that increasing efficiency required performance drop.

Both the external and internal optimization cases underline the maturity of adjoint-based optimization to reach desgin targets. The studied cases also highlight the bottlenecks of similar optimizations. Namely, the aerodynamic performance of waveriders represented by the lift-over-drag ratio could be improved only by decreasing the internal volume of the vehicle. Changes in the waverider geometry resulted in decreased lift and substantially decreased drag in every case. Considering the combustor, combustion efficiency was improved substantially by the optimization at the cost of higher total pressure drop. In short, efficiency was boosted by increasing losses inside the combustor.

The difference between baseline and optimized configurations is substantial but benefits are difficult to evaluate because of uncertainties associated with the employed RANS modelling framework. Future work

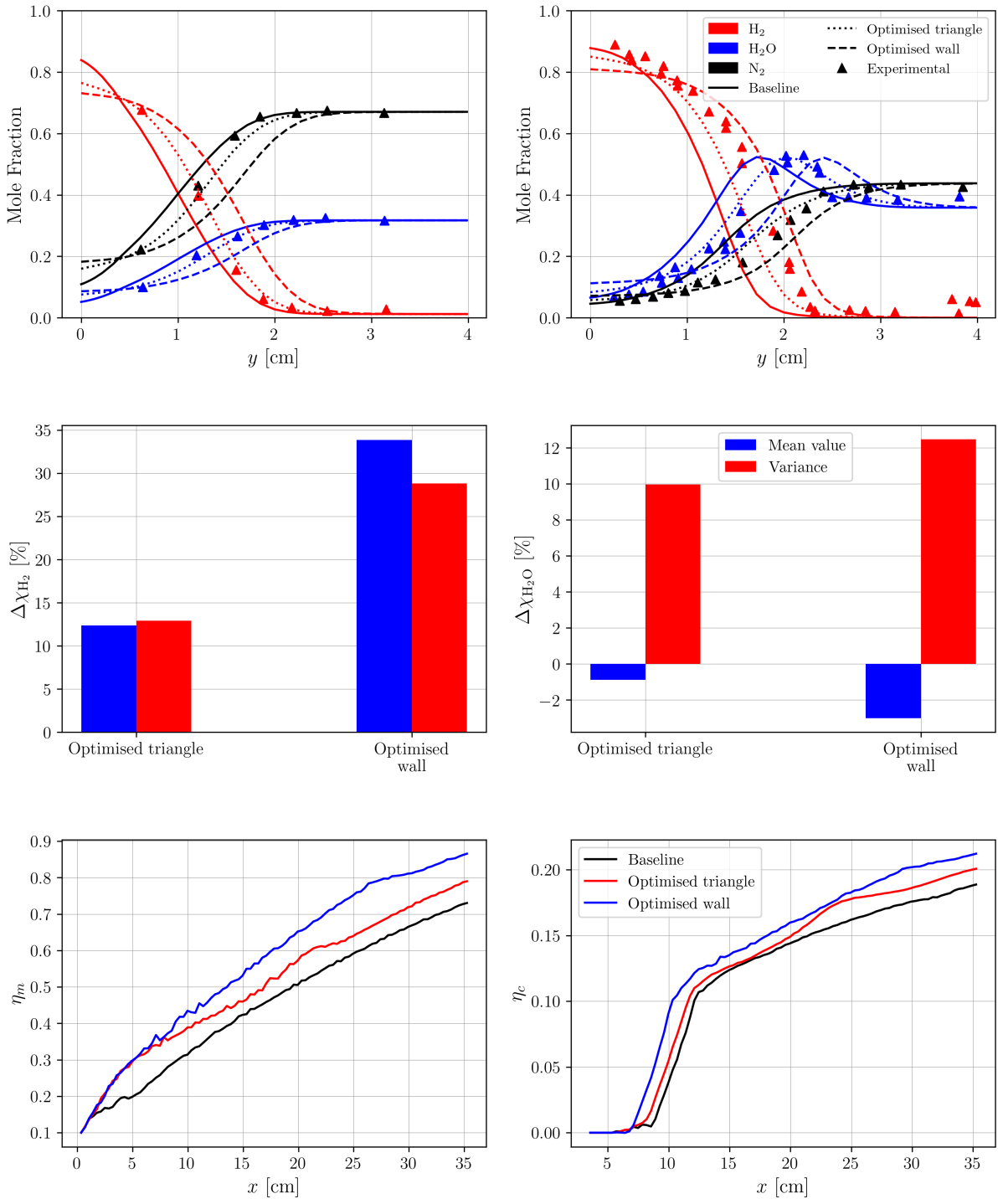

Fig 12. Comparison between the baseline and optimized cases for mixing (left) and reacting (right) stages of: outlet concentration (top row); mean and variance hydrogen concentration differences compared to the baseline case at the outlet (middle row); mixing and combustion efficiencies (bottom row).

might focus on quantifying and reducing such uncertainties and exploring more sophisticated direction and line search algorithms. Alternative parameterization of the geometry could be also considered for an increased control over the deformation.

References

[1] JD Anderson. *Hypersonic and high temperature gas dynamics, Second Edition*. AIAA, 2006.

[2] C Bruno and PA Czysz. *Future spacecraft propulsion systems: enabling technologies for space exploration*. Springer Science & Business Media, 2009.

[3] RW Guy. Hypersonic propulsion: Status and challenge. *AGARD, Hypersonic Combined Cycle Propulsion*, 1990.

[4] C McClinton. X-43-scramjet power breaks the hypersonic barrier: Dryden lectureship in research for 2006. In *44th AIAA aerospace sciences meeting and exhibit*, page 1, 2006.

[5] J Hank, J Murphy, and R Mutzman. The X-51A scramjet engine flight demonstration program. In *15th AIAA International Space Planes and Hypersonic Systems and Technologies Conference*, page 2540, 2008.

[6] J Steelant, A Mack, K Hannemann, and AD Gardner. Comparison of supersonic combustion tests with shock tunnels, flight and CFD. In *42nd AIAA/ASME/SAE/ASEE Joint Propulsion Conference and Exhibit*, Sacramento, California, July 2006.

[7] KG Bowcutt, A Paull, D Dolvin, and MK Smart. HIFiRE: An international collaboration to advance the science and technology of hypersonic flight. In *Proceedings of the 28th International Congress of the Aeronautical Sciences*, pages 2012–998. ICAS Secretariat RA Leiden, The Netherlands, 2012.

[8] P Roncioni, G Ranuzzi, M Marini, F Battista, and GC Rufolo. CFD aerothermodynamic characterization of the IXV hypersonic vehicle. In *7th European Symposium on Eerothermodynamics of Space Vehicles*, pages 9–12, 2011.

[9] S Paris, D Charbonnier, and D Tran. Experimental and numerical investigation of aerothermal characteristics of the IXV hypersonic vehicle. In *7th European Symposium on Aerothermodynamics*, volume 692, page 47, 2011.

[10] SA Berry, ML Mason, F Greene, R King, E Rieken, and K Basore. LaRC aerothermodynamic ground tests in support of BOLT flight experiment. In *AIAA Scitech 2019 Forum*, page 0091, 2019.

[11] BM Wheaton, DC Berridge, TD Wolf, DB Araya, RT Stevens, BE McGrath, BL Kemp, and DW Adamczak. Final design of the Boundary Layer Transition (BOLT) flight experiment. *Journal of Spacecraft and Rockets*, 58(1):6–17, 2021.

[12] JP Slotnick, A Khodadoust, J Alonso, D Darmofal, W Gropp, E Lurie, and DJ Mavriplis. CFD vision 2030 study: a path to revolutionary computational aerosciences. Technical report, NASA, 2014.

[13] A Cary, , J Chawner, E Duque, W Gropp, B Kleb, R Kolonay, E Nielsen, and B Smith. The CFD vision 2030 roadmap: 2020 status progress and challenges. Technical report, http://www.cfd2030.com/report, 2021.

[14] J RRA Martins, JJ Alonso, and JJ Reuther. High-fidelity aerostructural design optimization of a supersonic business jet. *Journal of Aircraft*, 41(3):523–530, 2004.

[15] KA Damm, RJ Gollan, PA Jacobs, MK Smart, S Lee, E Kim, and C Kim. Discrete adjoint optimization of a hypersonic inlet. *AIAA Journal*, 58(6):2621–2634, 2020.

[16] Siemens Digital Industries Software. Simcenter STAR-CCM+, version 2206. Siemens, 2023, https://www.plm.automation.siemens.com/global/en/products/simcenter/STAR-CCM.html.

[17] D Küchemann. *The aerodynamic design of aircraft*. American Institute of Aeronautics and Astronautics, Inc., 2012.

[18] JG Jones, KC Moore, J Pike, and PL Roe. A method for designing lifting configurations for high supersonic speeds, using axisymmetric flow fields. *Ingenieur-Archiv*, 37:56–72, 1968.

[19] ML Rasmussen. Waverider configurations derived from inclined circular and elliptic cones. *Journal of Spacecraft and Rockets*, 17(6):537–545, 1980.

[20] KG Bowcutt, JD Anderson, and D Capriotti. Numerical optimization of conical flow waveriders including detailed viscous effects. *Aerodynamics of Hypersonic Lifting Vehicles*, 1987.

[21] F Ding, J Liu, C Shen, Z Liu, S Chen, and X Fu. An overview of research on waverider design methodology. *Acta Astronautica*, 140:190–205, 2017.

[22] WO Landsberg, NN Gibbons, V Wheatley, MK Smart, and A Veeraragavan. Improving scramjet performance through flow field manipulation. *Journal of Propulsion and Power*, pages 1–13, 2017.

[23] J Urzay. Supersonic combustion in air-breathing propulsion systems for hypersonic flight. *Annual Review of Fluid Mechanics*, 50:593–627, 2018.

[24] MC Burrows and AP Kurkov. An analytical and experimental study of supersonic combustion of hydrogen in vitiated air stream. *AIAA Journal*, 11(9):1217–1218, 1973.

[25] S. Karl, K. Hannemann, A. Mack, and J. Steelant. CFD analysis of the HyShot II scramjet experiments in the HEG shock tunnel. In *15th AIAA International Space Planes and Hypersonic Systems and Technologies Conference*, page 2548, 2008.

[26] SN Skinner and H Zare-Behtash. State-of-the-art in aerodynamic shape optimisation methods. *Applied Soft Computing Journal*, 62:933–962, 2018.

[27] O Pironneau. On optimum design in fluid mechanics. *Journal of Fluid Mechanics*, 64(1):97–110, 1974.

[28] DN Srinath and S Mittal. An adjoint method for shape optimization in unsteady viscous flows. *Journal of Computational Physics*, 229(6):1994–2008, 2010.

[29] IS Kavvadias, EM Papoutsis-Kiachagias, G Dimitrakopoulos, and KC Giannakoglou. The continuous adjoint approach to the k-ω SST turbulence model with applications in shape optimization. *Engineering Optimization*, 47(11):1523–1542, 2015.

[30] J Lei and J He. Adjoint-based aerodynamic shape optimization for low Reynolds number airfoils. *Journal of Fluids Engineering, Transactions of the ASME*, 138(2):1–6, 2016.

[31] GLO Halila, JRRA. Martins, and KJ. Fidkowski. Adjoint-based aerodynamic shape optimization including transition to turbulence effects. *Aerospace Science and Technology*, 107:106243, 2020.

[32] R Rashad and DW Zingg. Aerodynamic shape optimization for natural laminar flow using a discrete-adjoint approach. *22nd AIAA Computational Fluid Dynamics Conference, June 1-20*, 2015.

[33] G Carpentieri, B Koren, and MJL van Tooren. Adjoint-based aerodynamic shape optimization on unstructured meshes. *Journal of Computational Physics*, 224(1):267–287, 2007.

[34] D Kapsoulis, K Tsiakas, X Trompoukis, V Asouti, and K Giannakoglou. A PCA-assisted hybrid algorithm combining EAs and adjoint methods for CFD-based optimization. *Applied Soft Computing Journal*, 73:520–529, 2018.

[35] J Luo, J Xiong, and F Liu. Aerodynamic design optimization by using a continuous adjoint method. *Science China: Physics, Mechanics and Astronomy*, 57(7):1363–1375, 2014.

[36] J Reuther and A Jameson. Supersonic wing and wing-body shape optimization using an adjoint formulation. *American Society of Mechanical Engineers, Fluids Engineering Division (Publication) FED*, 232(July):45–52, 1995.

[37] A Jameson, L Martinelli, and N A Pierce. Optimum aerodynamic design using the Navier-Stokes equations. *Theoretical and Computational Fluid Dynamics*, 10:213–237, 1998.

[38] ER Ashikhmina and PV Prosuntsov. Coupled CFD-based shape optimization of a wing of reusable space vehicle of tourist class. *IOP Conference Series: Materials Science and Engineering*, 709(2), 2020.

[39] DX Wang and L He. Adjoint aerodynamic design optimization for blades in multistage turbomachines-part i: Methodology and verification. *Journal of Turbomachinery*, 132, 4 2010.

[40] DX Wang, L He, YS Li, and RG Wells. Adjoint aerodynamic design optimization for blades in multistage turbomachines-part ii: Validation and application. *Journal of Turbomachinery*, 132, 4 2010.

[41] J Luo, J Xiong, F Liu, and Alstom Power. Three-dimensional aerodynamic design optimization of a turbine blade by using an adjoint method. *Article in Journal of Turbomachinery*, 2010.

[42] J Luo, I McBean, and F Liu. Optimization of endwall contours of a turbine blade row using an adjoint method. In *Turbo Expo: Power for Land, Sea, and Air, Vancouver, British Columbia, Canada, June 6–10*, volume 54679, pages 1335–1350, 2011.

[43] L Chen and J Chen. Aerodynamic optimization design for high pressure turbines based on the adjoint approach. *Chinese Journal of Aeronautics*, 28:757–769, 6 2015.

[44] JRRA Martins and GJ Kennedy. Enabling large-scale multidisciplinary design optimization through adjoint sensitivity analysis, 2019.

[45] T Dhert, T Ashuri, and JRRA Martins. Aerodynamic shape optimization of wind turbine blades using a Reynolds-averaged Navier–stokes model and an adjoint method. *Wind Energy*, 20:909–926, 5 2017.

[46] S He, E Jonsson, CA Mader, and JRRA Martins. Aerodynamic shape optimization with time spectral flutter adjoint. *AIAA Scitech 2019 Forum*, 2019.

[47] D Mavriplis, E Fabiano, and E Anderson. Recent advances in high-fidelity multidisciplinary adjoint-based optimization with the NSU3D flow solver framework. In *AIAA SciTech Forum - 55th AIAA Aerospace Sciences Meeting*. American Institute of Aeronautics and Astronautics Inc., 2017.

[48] M Méheut. Multidisciplinary adjoint-based optimizations in the madeleine project: Overview and main results. *AIAA AVIATION 2021 FORUM*, 2021.

[49] R Mosca. Adjoint-based passive optimization of a micro T-mixer. Master's thesis, Politecnico Di Milano, 2017.

[50] MF Eggl and PJ Schmid. Mixing by stirring: Optimizing shapes and strategies. *Physical Review Fluids*, 2022.

[51] E Helgason and S Krajnović. Implementation of an adjoint-based optimization with scalar transport. In *ASME 2014 International Mechanical Engineering Congress and Exposition*, 2014.

[52] J Yi, C Kim, and BJ Lee. Adjoint-based design optimization of vortex generator in an s-shaped subsonic inlet. *AIAA Journal*, 50:2492–2507, 11 2012.

[53] Q Chanzy, E Garnier, and R Bur. Optimization of a fluidic vortex generator's control in a transonic channel flow. *AIAA Journal*, 58(12):5216–5227, 10 2020.

[54] N Morita, T Tsuchiya, and H Taguchi. MDO of hypersonic waverider with trajectory-aero-structure coupling. In *23rd AIAA International Space Planes and Hypersonic Systems and Technologies Conference, 2020*. American Institute of Aeronautics and Astronautics Inc, AIAA, 2020.

[55] S Wei, D Chao, W Xiaopeng, and Z Yingtao. Aerodynamic design optimization of waverider-derived vehicle. *32nd Congress of the International Council of the Aeronautical Sciences, 2021*, pages 2–8, 2021.

[56] C Liu, F Qu, J Li, J Bai, C Liu, P Bai, and Z Qian. Aerodynamic optimization design of the vortex-shock integrated waverider in wide speed range. *Lixue Xuebao/Chinese Journal of Theoretical and Applied Mechanics*, 55(1):70–83, 2023.

[57] HL Kline, F Palacios, TD Economon, and JJ Alonso. Adjoint-based optimization of a hypersonic inlet. *American Institute of Aeronautics and Astronautics (AIAA)*, 6 2015.

[58] HL Kline, TD Economon, and JJ Alonso. Multi-objective optimization of a hypersonic inlet using generalized outflow boundary conditions in the continuous adjoint method. *54th AIAA Aerospace Sciences Meeting*, 2016.

[59] J Herrera. Waverider repository. https://github.com/j-herrera/waverider; Accessed: 2023-08-08.

[60] M Famada Vizcaino. Aerodynamic shape optimisation of hypersonic waveriders using CFD and adjoint-based method. Master's thesis, Cranfield University, 2023.

[61] MS Liou. Ten years in the making - AUSM-family. *AIAA Paper*, pages 2001–2521, 2001.

[62] A Simon Felix. Adjoint-based shape optimisation of hypersonic vehicles. Master's thesis, Cranfield University, 2023.

[63] MC Burrows and AP Kurkov. Analytical and experimental study of supersonic combustion of hydrogen in a vitiated airstream. Technical report, NASA Lewis Research Center, September 1973.

[64] C Rovira Sala. Optimisation of a generic supersonic hydrogen combustor. Master's thesis, Cranfield University, 2023.

[65] FR Menter, M Kuntz, and R Langtry. Ten years of industrial experience with the SST turbulence model. *Turbulence, heat and mass transfer*, 4(1), 2003.

[66] JJOE Hoste. *Scramjet combustion modeling using eddy dissipation model*. PhD thesis, University of Strathclyde, 2018.